Indonesian Journal of Chemical Research

http://ojs3.unpatti.ac.id/index.php/ijcr Indo. J. Chem. Res., 12 (3), 266-274, 2025

Iron Doped Calcium Manganese Oxide Cathode Materials for Aqueous Zinc Secondary Batteries

Gota Asano*, Yoshiyuki Kojima

Nihon University, 1-8, Kanda - Surugadai, Chiyoda - ku, Tokyo 101-8308, Japan
*Corresponding Author: ucsgo22001@g.nihon-u.ac.jp

Received: September 2024
Received in revised: December 2024
Accepted: January 2025
Available online: January 2025

Abstract

In recent years, zinc secondary batteries, which utilize a water-based electrolyte and offer high safety, have attracted attention as post-lithium-ion batteries. Zn has a high specific capacity (820 mAh/g) and a redox potential of -0.76 V (versus the standard hydrogen electrode) as a cathode. Furthermore, combining it with new cathode materials could significantly enhance performance. In particular, layered compounds containing manganese are inexpensive, widely used in industry, and considered promising candidates. This study synthesized calcium manganese oxide with a layered structure and investigated its potential as a cathode material for zinc secondary batteries. It is already known that $Ca_2Mn_3O_8$ has a layered structure and can be synthesized with a Mn/Ca atomic ratio ranging from 1.5 to 2.5. This research examined the effect of adding Fe and Al to this calcium manganese oxide on battery performance. When Fe was added, the battery capacity increased by 20%, reaching 177 mAh/g compared to the sample without Fe. This increase is believed to result from an increased interlayer distance, promoting the incorporation of structural water and enhancing ion conversion reactions during charge and discharge. However, adding Al was found to have no beneficial effect on battery performance.

Keywords: Calcium manganese oxide, Zinc secondary battery, Layered structure, Cathode, Iron.

INTRODUCTION

In recent years, efforts to achieve carbon neutrality by 2050 have gained momentum. The transportation sector, which accounts for approximately 18% of total CO_2 emissions, is a significant area, and there is a demand for the early conversion of gasoline-powered vehicles to electrification. Therefore, increasing the energy density and reducing the cost of lithium-ion batteries, the primary power source in electric vehicles, are crucial. Lithium-ion batteries, which have a high energy density and are lightweight, are ideal for extending the driving range of electric vehicles.

However, lithium-ion batteries face challenges such as the use of globally scarce materials, Li and Co, and significant CO_2 emissions during the manufacturing process, necessitating urgent research and development of post-lithium-ion alternatives (Ahmad et al., 2021; Ponrouch & Palacín, 2019; Pross-Brakhage et al., 2023; Walter et al., 2020).

Zinc (Zn) is known to be a metal with an exceptionally high energy density of 820 mAh/g among aqueous battery materials. However, although Zn has been used for a long time in primary batteries, such as alkaline manganese and air batteries, the research on optimal cathode materials for secondary batteries combined with Zn anodes is still in its early stages. Research is being conducted into electrolytic manganese dioxide for the cathode. Still, challenges remain, such as manganese changing into various forms during charge-discharge cycles and reacting with the zinc anode to form hetaerolite.

CV (Cyclic Voltammetry) measurements show zinc's strong oxidation (dissolution) peak. Still, since the reduction reaction is hardly seen (Febriyana & Setiarso, 2024), it indicates that zinc ions are constantly present in an unstable state on the surface of the anode. Although various studies have been conducted on cathodes for Zn-anode secondary batteries using weakly acidic or alkaline electrolytes, a cathode material for Zn anodes that can achieve both high capacity and long life has not yet been established (Wang et al., 2021).

Previous studies on manganese cathodes have utilized a two-electron reaction from $Mn^{4+} \rightleftharpoons Mn^{2+}$ to

achieve high capacity. It is believed that side reactions, dissolution of Mn^{2+}, and the deposition of passivation substances on the electrode surface during this reaction process are the causes of degradation. The crystal structure of manganese dioxide constantly changes due to charge and discharge reactions. Because it is unstable, defects occur within the structure, causing deterioration. Ca, one of the alkaline earth metals, is relatively stable even in alkaline aqueous solutions. It was considered that mixing it with manganese oxides could compensate for structural defects. $Ca_2Mn_3O_8$ has a layered structure and can be synthesized with an Mn/Ca atomic ratio in the range of 1.5–2.5 (Gagrani & Tsuzuki, 2019; Najafpour et al., 2013; Stimpson et al., 2020; Stimpson et al., 2020). As a battery material, it has been reported to exhibit a specific capacity of 210 mAh/g as a calcium manganese oxide ($Ca_2Mn_3O_8$) electrode in a 9 M KOH alkaline solution (Sugawara et al., 1991). Additionally, it has been reported that calcium manganate is helpful as a hydrogen storage material in a 2 M KOH alkaline solution (Samimi et al., 2023).

Previous reports suggest a composition range of Mn/Ca atomic ratio 1.5 to 2.5 is applicable. Furthermore, an evaluation of a zinc secondary battery using $Ca_2Mn_3O_8$ as the cathode has shown a discharge capacity of 368 mAh/g when a mixed electrolyte of Zn $(CF_3SO_3)_2$ and $Mn(CF_3SO_3)_2$ has been used (Wang et al., 2021). This study used layered calcium manganese oxide, a low-cost and reliable material, as a novel cathode material for aqueous zinc-anode secondary batteries. The relationship between the intercalation reactions utilizing its structure and the characteristics of Zn secondary batteries was investigated. In addition, the effects of adding Fe or Al during the synthesis of calcium manganese oxide on the material properties and battery characteristics were examined. It is already known that doping the ternary NCM (nickel manganese cobalt oxides) cathode, used in lithium-ion batteries with Fe or Al, stabilizes its structure. This study evaluated whether a similar effect could be obtained with aqueous calcium manganate cathodes.

METHODOLOGY

Materials and Instrumentals

Calcium manganese oxide (CMO) was synthesized using calcium chloride (99.0% purity; Kanto Kagaku) and manganese chloride tetrahydrate (99.0% purity; Kanto Kagaku). The alkaline solution used for co-precipitation contained 86.0% potassium hydroxide (Kanto Kagaku). Iron chloride tetrahydrate (Kanto Kagaku) and aluminium chloride hexahydrate (Kanto Kagaku) were used as additives in CMO.

The samples were characterized by thermal analysis (TG–DTA), Fourier transform infrared spectroscopy (FT-IR), X-ray diffraction (XRD), and scanning electron microscopy (SEM). The electrochemical properties were evaluated using cyclic voltammetry (CV).

Procedure

Electrode fabrication

Calcium chloride and manganese chloride were weighed to achieve an arbitrary Mn/Ca atomic ratio, (molar ratio of Mn and Ca atoms) and a suspension was prepared using pure water. The mixture was stirred with 2 mol·dm^{-3} potassium hydroxide solution at 80 ^{o}C for one hour (the KOH / (Mn+Ca) molar ratio was 2.0). The precursor thus generated was washed and filtered with hot water at 80 ^{o}C (using 1 dm^3 of pure water per 15 g of the sample), dried at 70 ^{o}C, and then calcined at 700 ^{o}C for two hours to obtain the CMO sample. Additionally, to investigate the effect of Fe or Al addition, CFMO (Fe-doped CMO) and CAMO (Al-doped CMO) samples were synthesized by adding iron chloride and aluminium chloride, respectively, to the suspension of calcium chloride and manganese chloride in arbitrary atomic ratios.

Preparing the cathode composite electrodes, The samples were mixed with Ketjen black and polyvinylidene fluoride (PVdF) powder, dissolved in N-methyl-2-pyrrolidone (NMP) in a ratio of 1:10 by weight, and stirred. The mixture was then loaded onto a nickel foam substrate (Niraco), dried at 80 ^{o}C, and rolled. The electrodes had a thickness of 0.3 mm and an areal weight of 0.03 g/cm^2. Preparing the composite electrode required optimizing the type of carbon and binder to suit the coating process (Wahyuni et al., 2021) and a combination suitable for the Ni form was chosen.

Laminated cell fabrication

The configuration of the zinc secondary battery evaluated in this study is shown in Figure 1. The positive electrode and a metal zinc plate (Nirako, purity 99.99%, thickness 0.5 mm, area 16 cm^2) were thermally fused and covered with a polypropylene non-woven fabric separator. For the electrolyte, an 8 mol·dm^{-3} potassium hydroxide solution (saturated with zinc oxide: ZnO 0.5 mol/dm^3) was used to fabricate the laminated battery, and testing was conducted.

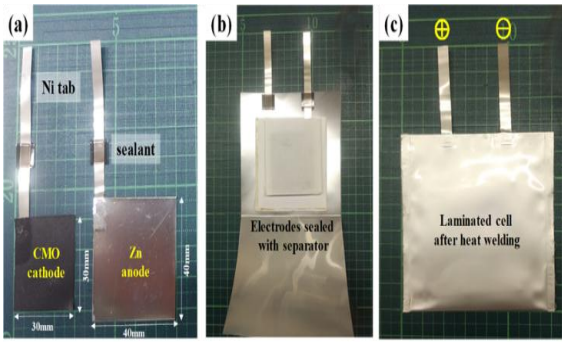

Figure 1. Laminated battery configuration for testing of (a) electrodes, (b) stacked electrodes, and (c) laminated cell.

RESULTS AND DISCUSSION

Evaluation of CMO Samples

Two methods are available for synthesizing calcium manganate: the dry method, which uses calcium oxide and manganese dioxide as starting materials, which are ground, mixed, and fired, and the wet method, in which calcium nitrate and manganese nitrate solutions are mixed.

However, in this study, cheaper chlorides were used as raw materials, and the precipitation method, which allowed for more homogeneous and low-temperature firing than the dry method, was used for the synthesis. Figure 2 shows the Mn/Ca atomic ratio change immediately after firing. Compared to the Mn/Ca atomic ratio during synthesis, the composition after firing showed a tendency for the Mn content to increase relative to Ca. Because no peaks of calcium hydroxide or calcium carbonate were confirmed in the XRD pattern of the fired samples, it was presumed that the unreacted calcium fraction was discharged during the filtration.

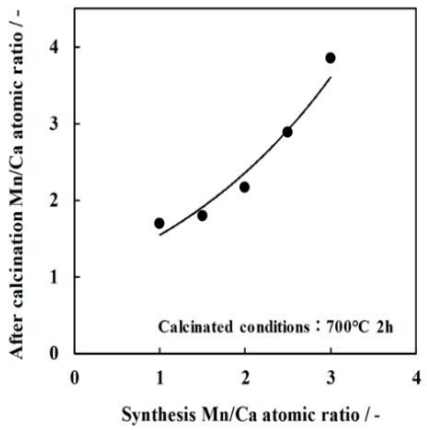

Figure 2. Mn/Ca atomic ratio after synthesis.

Figure 3 shows the XRD pattern of CMO synthesized with an Mn/Ca atomic ratio of 1.0–3.0. As the Mn/Ca atomic ratio increased, the diffraction peaks increased, and a layered structure was confirmed for $Ca_2Mn_3O_8$ with Mn/Ca atomic ratios of 1.5–2.5 (Han et al., 2013; Tham et al., 2021).

At Mn/Ca atomic ratios of 1.0 and 3.0, the peak intensity around 17° indicated that the interlayer was hardly observed. The increase in the Mn/Ca atomic ratio after firing compared with that during synthesis is thought to be because of the coexistence of $Ca_2Mn_3O_8$ and $CaMn_3O_6$, as seen from the X-ray diffraction results (Hadermann et al., 2006).

Few studies have reported the characteristics of layered calcium manganate for Mn/Ca atomic ratios in the range of 1.5–2.5. When $Ca_2Mn_3O_8$ is formed, it does not necessarily show a high purity Mn/Ca atomic ratio of 1.5; in an alkaline solution, if there is no excess Mn, owing to the influence of unstable Mn oxides, the target product is unlikely to be achieved.

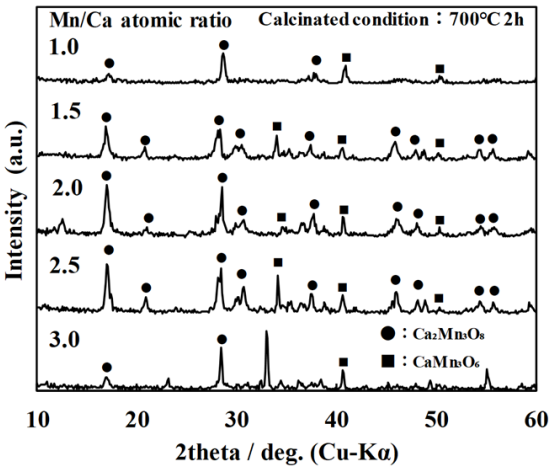

Figure 3. XRD patterns of CMO samples with Mn/Ca atomic ratios varying from 1.0 to 3.0.

Table 1 shows the relationship between the firing conditions for each Mn/Ca atomic ratio and the capacity of the CMO/Zn secondary battery. At this time, charging was performed at a rate of 0.1 C up to an upper voltage of 1.65 V, and discharging was performed at 0.1 C in the same manner down to a termination voltage of 0.5 V (current density: 0.7 mA/cm²). The battery capacity was the largest (142 mAh/g CMO) at an Mn/Ca atomic ratio of 2.0, with the optimal firing condition being 700 °C for 2 h.

Table 1. CMO/Zn battery test results using CMO synthesized with varying calcination conditions.

Mn/Ca atomic ratio	Calcinated Conditions	Battery Capacity (mAh/g) ※1	Capacity after 15 cycles (mAh/g) ※1
1.0	700 ℃ 2h	14	14
1.5		110	15
2.0	550 ℃ 2h	67	0
	700 ℃ 2h	*142*	*39*
	750 ℃ 5h	72	10
	850 ℃ 2h	61	23
	950 ℃ 5h	8	―
2.5	700 ℃ 2h	77	17
3.0		50	29

※1） Test Conditions ;
Charge : 0.1C CC1.65V / Discharge : 0.1C to 0.5V at 25 ℃

Figure 4 shows the XRD patterns obtained at each firing temperature. As mentioned above, at an Mn/Ca atomic ratio of 2.0, the battery capacity tended to decrease when firing continued for more than 3 hours at the low temperature side of 550 ℃ or the high temperature side above 800 ℃. From the X-ray diffraction results, it was inferred that at around 650–750 ℃, the layered structure of $Ca_2Mn_3O_8$ was maintained, and ion conductivity and charge-discharge reactions progressed efficiently within the structure (Jinjun et al., 2020). Hereafter, the samples to be synthesized are compared under firing conditions of 700 ℃ for 2 hours.

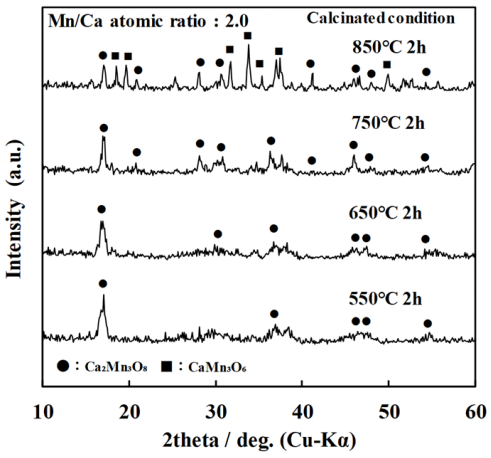

Figure 4. XRD patterns of CMO samples synthesized at different calcination temperatures.

Evaluation of CFMO and CAMO Samples

To further increase the capacity of manganese oxides, comparative evaluations were conducted on alkaline earth metals other than Ca. Even among elements in the same group as Ca, the characteristics can vary significantly when combined with Mn. There are reports on Mn compounds using Mg, Sr, and Ba (Hong et al., 2019; Ling & Zhang, 2017; Zhang et al., 2017). Additionally, in manganese compounds using Ba, Mn changes to various forms from Mn^{4+} to Mn^{7+} (Akbari et al., 2021; Kwon et al., 2008)

In the case of Ca, compounds with Mn having a valency of +2 to +4 are formed, indicating stable manganese oxide formation. Manganese oxides substantially depend on dopant ions because they affect the crystal phase, crystal structure, and average atomic valence. It has been reported that Ca forms a compound with α-MnO_2, while Mg forms a compound with γ-MnO_2 (Randhir et al., 2019)

Furthermore, various synthesis methods, such as hydrothermal synthesis, ion exchange, electrodeposition, and firing, significantly affect the electrochemical properties. In this study, the battery capacity of Mn compounds with Ca was the highest among the alkaline earth metals (Mg:27, Sr:76, Ba:69 mAh/g). This condition is thought to be due to the high affinity with calcium in synthesizing manganese compound precursors by the precipitation method in the high-pH region, which can form a more stable layered structure (Ren et al., 2022).

On the other hand, studies have suggested that adding rare earth elements to calcium manganese oxide can enhance the crystal structure (Linh et al., 2010) and that adding calcium to manganese ferrite improves the catalytic activity (Iqbal et al., 2020). Additionally, the crystal structure of ternary lithium-ion cathode materials, such as nickel–manganese–cobalt (NMC) oxides, is stabilized by adding Fe or Al (Jeong et al., 2021; Kim, et al., 2017; Park et al., 2020).

Based on these facts, it is suggested that partially substituting the compounds forming layered structures with metal oxides can further increase the battery capacity. In this study, the effects of adding Fe and Al were investigated.

Figure 5 shows the XRD patterns of the calcium manganese oxide samples synthesized with Fe and Al additions. The diffraction peak of $Ca_2Mn_3O_8$ was observed even with Fe and Al added (Figure 5 (a)). In this case, the amount of each addition was set and evaluated at Fe/(Fe+Mn) atomic ratio of 0.2 for CFMO and Al/(Al+Mn) ratio of 0.2 for CAMO. As a comparison, in the X-ray diffraction of CFMO, set at Fe/(Fe+Mn) atomic ratios of 0.1 and 0.5, the peak around 17 °(2θ) indicated that the interlayer decreased compared to that at the atomic ratio of 0.2; therefore, the investigation was conducted at addition amounts of 0.1 and 0.5. The peaks at approximately 17° for CMO, CFMO, and CAMO are presented in a magnified view for clarity in Figure 5(b); compared with CMO, the peaks for CFMO and CAMO shifted to lower angles by approximately 0.1°, indicating that the interlayer distance increased with the addition of Fe and Al. In the case of Al addition, it was also confirmed that this peak was broader than Fe addition's.

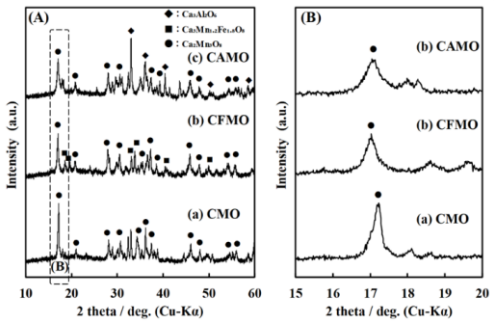

Figure 5. XRD patterns of (a) CMO, CFMO and CAMO ; (b) an expanded view of the diffraction peak for CMO, CFMO and CAMO.

Figure 6 shows the TG–DTA results of these samples. In CMO and CFMO, significant weight changes and exothermic peaks were observed in the temperature region above 800 ℃. CMO, with a $CaMnO_3$ composition, is also used as a thermoelectric conversion material and particularly dense sintered bodies are generated around 900 ℃ (Ohtaki et al., 1995). In this study, the aim is to incorporate Zn^{2+} eluted from the zinc anode and K^+ and OH^-in the electrolyte into the cathode structure to induce reversible intercalation, and thus, perovskite-type structures such as thermoelectric conversion materials are not considered suitable. Therefore, it is necessary to confine more structural water between layers and maintain it within the structure. In the case of CAMO, dehydration is observed at a relatively early stage, and no significant weight change is observed around 800 ℃.

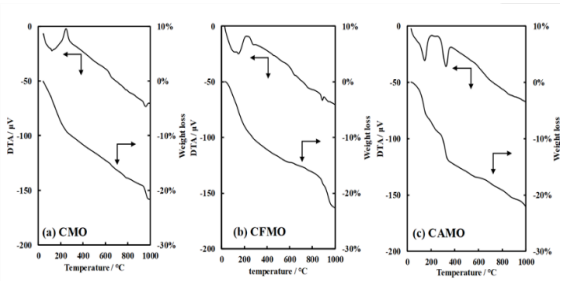

Figure 6. TG／DTA curves for: (a) CMO, (b) CFMO and (c) CAMO.

Figure 7 shows the FT-IR spectra. In the case of calcium manganese oxide, Ca–Mn metal oxide bonds are observed around 500–600 cm^{-1}. It was confirmed that the absorption spectrum intensity of CAMO was lower than that of CMO and CFMO. This result suggests that the crystal structure becomes unstable when Al is doped. Additionally, it was observed that the intensity around 3400 cm^{-1} indicating H_2O and OH in CFMO was larger compared to CMO and CAMO. This is thought to be because the space between the CFMO layers expands, allowing it to retain a large amount of structural water.

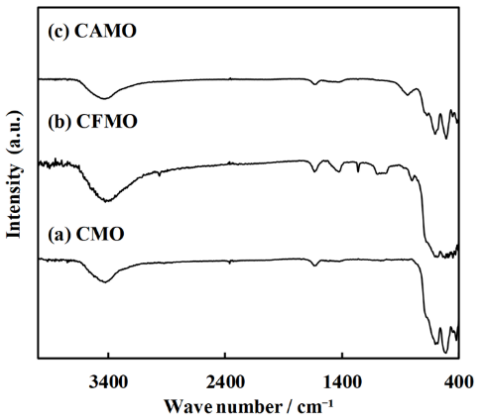

Figure 7. FT-IR spectra of: (a) CMO, (b) CFMO, and (c) CAMO.

Figure 8 shows the SEM results. Although CMO was an aggregate of plate-like crystals that became partially pasty, CFMO contained many fibrous crystals. As a result of EDS observation, Fe was not present in large amounts in the fibre portion. When Mn and Fe coexist, Fe is more reactive, and complex

formation proceeds more rapidly (La Harimu et al., 2020), so it is inferred that a different crystal structure was formed compared to CMO. In the case of CAMO, many pasty crystals were mixed with long rod-like crystals. Additionally, the amount of Fe decreased compared with the input atomic ratio, whereas the amount of Al tended to increase.

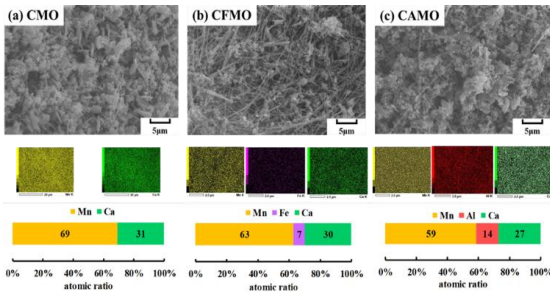

Figure 8. SEM images and EDS results for: (a) CMO; (b) CFMO and (c) CAMO.

Figure 9 shows the CV curves of each sample. Compared with CMO, CFMO showed an increasing trend in the redox peaks, whereas CAMO showed a decreasing trend. In particular, the increase in the reduction peaks in CFMO suggests the possibility of incorporating many ions into the interlayers during the oxidation (dissolution) of the zinc electrode.

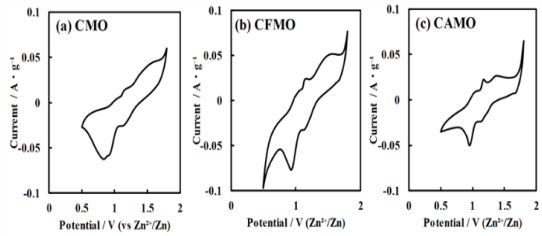

Figure 9. Cyclic voltammograms for (a) CMO, (b) CFMO and (c) CAMO.

Figure 10 shows the capacity of the Zn secondary batteries using each sample as the cathode. While CMO had a capacity of 140 mAh/g, CFMO was confirmed to extend the battery capacity by more than 20% to 177 mAh/g. On the other hand, CAMO had a capacity of 50 mAh/g, which was less than half the capacity of CMO. It was inferred that the increase in capacity in CFMO was due to factors such as the increase in the interlayer distance and the amount of structural water present between the layers. In the case of the CAMO, although the interlayer distance increased, the weak Ca–Mn bonds and weak structural water retention observed in the TG–DTA results did not increase capacity.

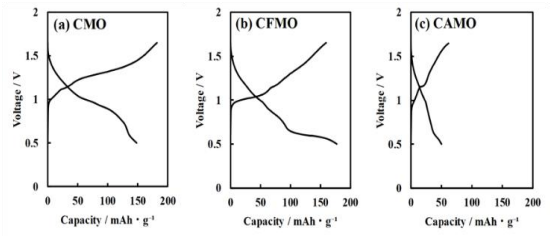

Anode Zn; Electrolyte 8M KOH (ZnO sat.);

Conditions Charge: 0.1 C CC 1.65 V / Discharge: 0.1 C to 0.5 V at 25 ℃.

Figure 10. Laminated zinc secondary battery test results for: (a)CMO, (b) CFMO, and (c) CAMO.

Table 2 compares battery capacities at sintering temperatures of 550 ℃,700 ℃, and 850 ℃. CFMO achieved almost the same capacity at 700 ℃ and 850 ℃. In contrast, at 550 ℃, the battery capacity decreased by 30% compared to the 700 ℃ sintered product. For CAMO, the capacity at 700 ℃ tended to be larger than 850 ℃.

Table 2. Battery test results using CFMO and CAMO synthesized with varying calcination conditions.

	Atomic ratio	Calcinated Conditions	Battery Capacity (mAh/g)※1
	Fe / (Fe + Mn)		
CFMO	0.1	550 ℃ 2h	139
		700 ℃ 2h	78
	0.2	550 ℃ 2h	129
		700 ℃ 2h	177
		850 ℃ 2h	181
	Al / (Al + Mn)		
CAMO	0.2	700 ℃ 2h	50
		850 ℃ 2h	64

※1）Test Conditions ; Charge : 0.1C CC1.65V / Discharge : 0.1C to 0.5V at 25 ℃

Figure 11 shows the results of the charge-discharge cycle tests. Here, the open circuit voltage (OCV) immediately after battery assembly is approximately 1.2-1.4V. At this time, the state is such that the manganese in the positive electrode is Mn^{4+}, and the test starts from the discharge because the battery is in a charged state. In the case of CMO, there is a tendency for the charge capacity to decrease rapidly with cycling rapidly. In contrast, in the case of CFMO, stable charge-discharge is maintained from the initial stage, and the cumulative capacity up to 15 cycles was the highest. After a few cycles, the samples fired at 850 ℃ with the same capacity showed significant deviations in the charge-discharge curve,

resulting in a markedly different cycling characteristic than those fired at 700 °C. This result is thought to be because, like CMO, firing at 850 °C led to the formation of $CaMn_3O_6$ and structural instability. On the other hand, CAMO was confirmed to deteriorate rapidly. Compared to different samples, it has a lower overvoltage during charging, leading to a significant decrease in charge-discharge efficiency due to oxygen evolution (Meng et al., 2022; Pathreeker et al., 2020).

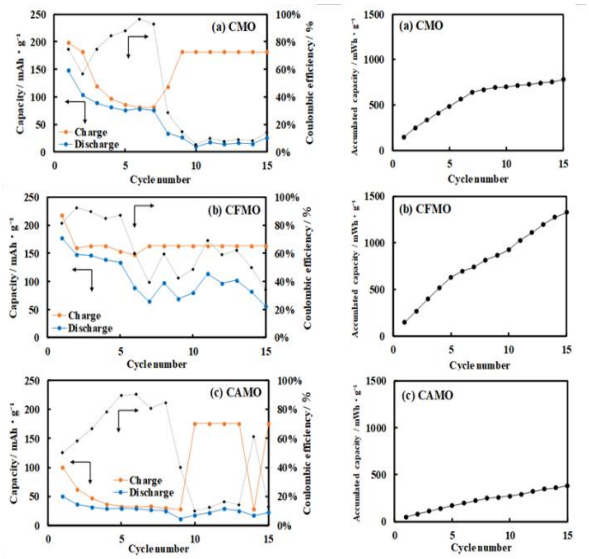

Anode Zn; Electrolyte 8M KOH (ZnO sat.);

Conditions Charge: 0.1 C CC 1.65 V / Discharge: 0.1 C to 0.5 V at 25 °C.

Figure 11. Laminated zinc secondary battery cycle test results for: (a)CMO; (b) CFMO and (c) CAMO.

Figure 12 shows the charge-discharge cycle characteristics of CFMO when the charge-discharge rate is doubled. It was confirmed that increasing the rate reduces the discharge capacity by 60%, but the capacity retention rate improves by about 10%. Compared to low-rate charging and discharging, performing high-rate charging and discharging results in a shallower charge-discharge depth and extended cycle characteristics. This showed a similar trend to that observed in previously studied MnO_2 cathodes.

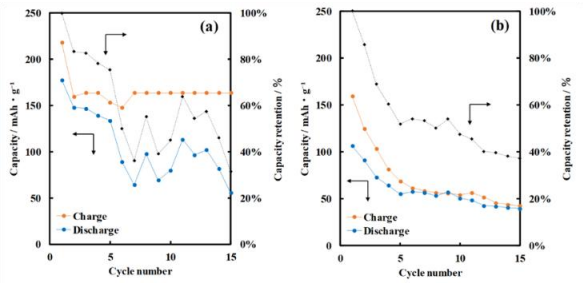

Current density ; (a) 0.7mA/cm²; (b) 1.4mA/cm²

Anode Zn; Electrolyte 8M KOH (ZnO sat.);

Conditions Charge: CC 1.65 V / Discharge: Cut off 0.5 V at 25 °C.

Figure 12. Laminated CFMO/Zn secondary battery cycle test results.

CONCLUSION

In this study, a close relation was observed between the crystal structure of calcium manganate, synthesized by co-precipitation from chlorides, and the capacity of Zn secondary batteries, mainly when the composition had a layered structure, resulting in the highest battery capacity. Thus, ions moved reversibly between the layers within the crystal structure during charging and discharging, accompanied by electron exchange reactions. It was confirmed that calcium manganate formed $Ca_2Mn_3O_8$ within a narrow range of 1.5–2.5 Mn/Ca atomic ratios, along with the presence of $CaMn_3O_6$. In the zinc secondary batteries of the laminate type, the capacity was the largest at an Mn/Ca atomic ratio of 2.0, reaching 140 mA/g. Further, adding iron to CMO increased the battery capacity by about 20% (177 mAh/g) and improved the initial cycle stability. The improvement in cycle characteristics is because the addition of iron suppresses the degradation of the calcium manganese oxide during charge-discharge cycles and maintains a stable crystal structure. Compared with Al, Fe was found to be more effective in a solid solution with calcium manganate. The optimal Fe/ (Fe + Mn) atomic ratio and firing temperature were 0.20 and 700 °C, respectively. Verifying the potential of zinc secondary batteries to attain a specific energy density by utilizing cost-effective minerals plentiful in the Earth's crust rather than relying on expensive materials such as nickel and cobalt is essential for developing post-lithium-ion batteries. Future research can focus on selecting optimal applications and improving the long-term reliability of these batteries.

REFERENCES

Ahmad, Y., Colin, M., Gervillie-Mouravieff, C., Dubois, M., & Guérin, K. (2021). Carbon in lithium-ion and post-lithium-ion batteries: Recent features. *Synthetic Metals*, *280*(116864).

Akbari, E., Alavi, S. M., Rezaei, M., & Larimi, A. (2021). Barium promoted manganese oxide catalysts in low-temperature methane catalytic combustion. *International Journal of Hydrogen Energy*, *46*(7), 5181–5196.

Febriyana, A., & Setiarso, P. (2024). Fabrication of Carbon Paste Electrode Modified with ZnO Nanoparticles and Nanobentonite for Analysis of Bisphenol A by Cyclic Voltammetric. *Indonesian Journal of Chemical Research*, *12*(2), 119–128.

Gagrani, A., & Tsuzuki, T. (2019). Calcium manganese oxides as biomimetic catalysts in energy applications: A short review. *Chemical Engineering Science*, *194*, 116–126.

Hadermann, J., Abakumov, A. M., Gillie, L. J., Martin, C., & Hervieu, M. (2006). Coupled Cation and Charge Ordering in the CaMn3O6 Tunnel Structure. *Chemistry of Materials*, *18*(23), 5530–5536.

Han, X., Zhang, T., Du, J., Cheng, F., & Chen, J. (2013). Porous calcium–manganese oxide microspheres for electrocatalytic oxygen reduction with high activity. *Chem. Sci.*, *4*(1), 368–376.

Hong, J., Aphale, A. N., Heo, S. J., Hu, B., Reisert, M., Belko, S., & Singh, P. (2019). Strontium Manganese Oxide Getter for Capturing Airborne Cr and S Contaminants in High-Temperature Electrochemical Systems. *ACS Applied Materials & Interfaces*, *11*(38), 34878–34888.

Iqbal, Z., Sadiq, S., Sadiq, M., Ali, M., Saeed, K., Ur Rehman, N., … Shah, M. H. (2020). Synergetic Effect of Calcium Doping on Catalytic Activity of Manganese Ferrite: DFT Study and Oxidation of Hydrocarbon. *Crystals*, *10*(4).

Jeong, S., Park, S., Beak, M., Park, J., Sohn, J.-S., & Kwon, K. (2021). Effect of Residual Trace Amounts of Fe and Al in Li[Ni1/3Mn1/3Co1/3]O2 Cathode Active Material for the Sustainable Recycling of Lithium-Ion Batteries. *Materials*, *14*(9).

Jinjun, H., Xihong, L., Haozhe, Z., & Xiaoqing, L. (2020). Enhancing Zn^{2+} Storage Capability of Cobalt Manganese Oxide by *In-Situ* Nanocarbon Coating. *Acta Chimica Sinica*, *78*(10), 1069.

Kim, U.-H., Myung, S.-T., Yoon, C. S., & Sun, Y.-K. (2017). Extending the Battery Life Using an Al-Doped Li[Ni0.76Co0.09Mn0.15]O2 Cathode with Concentration Gradients for Lithium Ion Batteries. *ACS Energy Letters*, *2*(8), 1848–1854.

Kwon, D.-K., Akiyoshi, T., Lee, H., & Lanagan, M. T. (2008). Synthesis and Electrical Properties of Stabilized Manganese Dioxide (α-MnO2) Thin-Film Electrodes. *Journal of the American Ceramic Society*, *91*(3), 906–909.

La Harimu, L. H., Haetami, A., Sari, C., Haeruddin, H., & Nurlansi, N. (2020). Comparison of Spray Aeration Ability (Spray) with Adsorption Method Using Adsorbent Powder Cocoa Rind to Reduce Iron and Manganese Levels in Dug Well Water. *Indonesian Journal of Chemical Research*, *8*(2).

Ling, C., & Zhang, R. (2017). Manganese Dioxide As Rechargeable Magnesium Battery Cathode. *Frontiers in Energy Research*, *5*.

Linh, N. H., Trang, N. T., Cuong, N. T., Thao, P. H., & Cong, B. T. (2010). Influence of doped rare earth elements on electronic properties of the R0.25Ca0.75MnO3 systems. *Computational Materials Science*, *50*(1), 2–5.

Meng, Z., Reupert, A., Tang, Y., Li, Z., Karkera, G., Wang, L., … Zhao-Karger, Z. (2022). Long-Cycle-Life Calcium Battery with a High-Capacity Conversion Cathode Enabled by a Ca2+/Li+ Hybrid Electrolyte. *ACS Applied Materials & Interfaces*, *14*(49), 54616–54622.

Najafpour, M. M., Leonard, K. C., Fan, F.-R. F., Tabrizi, M. A., Bard, A. J., King'ondu, C. K., … Allakhverdiev, S. I. (2013). Nano-size layered manganese–calcium oxide as an efficient and biomimetic catalyst for water oxidation under acidic conditions: Comparable to platinum. *Dalton Trans.*, *42*(14), 5085–5091.

Ohtaki, M., Koga, H., Tokunaga, T., Eguchi, K., & Arai, H. (1995). Electrical Transport Properties and High-Temperature Thermoelectric Performance of (Ca0.9M0.1)MnO3 (M = Y, La, Ce, Sm, In, Sn, Sb, Pb, Bi). *Journal of Solid State Chemistry*, *120*(1), 105–111.

Park, Y., Kim, Y., Chang, H., Won, S., Kim, H., & Kwon, W. (2020). Biocompatible nitrogen-doped carbon dots: Synthesis,

characterization, and application. *Journal of Materials Chemistry B*, *8*(39), 8935–8951.

Pathreeker, S., Reed, S., Chando, P., & Hosein, I. D. (2020). A study of calcium ion intercalation in perovskite calcium manganese oxide. *Journal of Electroanalytical Chemistry*, *874*, 114453.

Ponrouch, A., & Palacín, M. R. (2019). Post-Li batteries: Promises and challenges. *Philosophical Transactions of the Royal Society A: Mathematical, Physical and Engineering Sciences*, *377*(2152), 20180297. https://doi.org/10.1098/rsta.2018.0297

Pross-Brakhage, J., Fitz, O., Bischoff, C., Biro, D., & Birke, K. P. (2023). Post-Lithium Batteries with Zinc for the Energy Transition. *Batteries*, *9*(7), 1–20.

Randhir, K., King, K., Rhodes, N., Li, L., Hahn, D., Mei, R., … Klausner, J. (2019). Magnesium-manganese oxides for high temperature thermochemical energy storage. *The Journal of Energy Storage*, *21*, 599–610.

Ren, Z., Tang, Z., Chen, X., Li, Z. H., & Lei, G. (2022). Exploration of Calcium-Doped Manganese Monoxide Cathode for High-Performance Aqueous Zinc-Ion Batteries. *Energy & Fuels*, *36*.

Samimi, F., Ghiyasiyan-Arani, M., Salavati-Niasari, M., & Alwash, S. W. (2023). A study of relative electrochemical hydrogen storage capacity of active materials based on Zn3Mo2O9/ZnO and Zn3Mo2O9/ZnMoO4. *International Journal of Hydrogen Energy*, *48*(27), 10070–10080.

Stimpson, L. J. V., Etherdo-Sibley, K. J. W., Ridley, C. J., Bull, C. L., & Arnold, D. C. (2020). Phase stability of the layered oxide, Ca2Mn3O8; probing interlayer shearing at high pressure. *Mater. Adv.*, *1*(6), 1841–1848.

Sugawara, M., Iura, S., & Matsuki, K. (1991). Discharge Characteristics of $Ca_2Mn_3O_8$ and Its Modified Oxides in Alkaline Solutions. *Denki Kagaku Oyobi Kogyo Butsuri Kagaku*, *59*(11), 988–991.

Tham, N. N., Ge, X., Yu, A., Li, B., Zong, Y., & Liu, Z. (2021). Porous calcium–manganese oxide/carbon nanotube microspheres as efficient oxygen reduction catalysts for rechargeable zinc–air batteries. *Inorg. Chem. Front.*, *8*(8), 2052–2060.

Wahyuni, W. T., Putra, B. R., Fauzi, A., Ramadhanti, D., Rohaeti, E., & Heryanto, R. (2021). A Brief Review on Fabrication of Screen-Printed Carbon Electrode: Materials and Techniques. *Indo. J Chem. Res.*, *8*(3), 210–218.

Walter, M., Kovalenko, M. V., & Kravchyk, K. V. (2020). Challenges and benefits of post-lithium-ion batteries. *New Journal of Chemistry*, *44*(5), 1677–1683.

Wang, L., Cao, Z., Zhuang, P., Li, J., Chu, H., Ye, Z., Ye, M. (2021). Electrochemical Injection Oxygen Vacancies in Layered Ca2Mn3O8 for Boosting Zinc-Ion Storage. *ACS Applied Materials & Interfaces*, *13*(11), 13338–13346.

Zhang, H., Ye, K., Shao, S., Wang, X., Cheng, K., Xiao, X., … Cao, D. (2017). Octahedral magnesium manganese oxide molecular sieves as the cathode material of aqueous rechargeable magnesium-ion battery. *Electrochimica Acta*, *229*, 371–379.